QATNU Shutter Phase VI

Matched Histories, Native Matter Control, Outgoing Modes, and MPO-Krylov Propagation

Computational experiment report

19 June 2026

Abstract

This report closes the next integration tier of the autonomous QATNU/SRQID shutter benchmark. It replaces static scattering references by references with matched switching histories, embeds the shutter gate directly in two ordinary matter qubits through the standard frustration projector, tests that native matter gate under generic perturbations, compares independent Hilbert-space regulators, constructs outgoing positive-frequency modes on one undoubled Gaussian chain, reconstructs a finite native outgoing-mode density matrix, and builds a compact matrix-product-operator Krylov solver. Matched histories reduce the previous far-right local-algebra mismatch by a factor 4.59. On the cutoff-free chain, matched outgoing mode and covariance reduce the photon-side Weyl mismatch by a factor 45.8 relative to a permanently open reference. A two-qubit frustration gate drives transmission 0.88894 with resolved controller backaction and conserved total energy. A bond-dimension-four MPO reproduces the exact small-system propagator to packet fidelity squared 0.999999999944. The report retains the unresolved long-time, long-chain tensor-network limit as an explicit bottleneck.

Principal conclusion. The mismatch found in Phase V was largely a reference-state problem, not a failure of the autonomous shutter. Matching the switching history and outgoing positive-frequency mode removes most of it. The same mechanism now works with a native two-matter-qubit frustration gate and with independently converged edge-register regulators. A compact MPO-Krylov formulation is exact at small size, but long-time, long-chain convergence is not yet established.

1 Scope and decisive questions

Phase V showed that a protected matter clock, square-root edge ladders, and a direct edge–edge bilinear can be combined under one fixed Hamiltonian. It also produced a negative result: the final controller label alone did not make an outgoing block equivalent to a permanently open reference. The present phase asks:

1. Does a reference with the correct switching history resolve that mismatch?
2. Can ordinary QATNU matter qubits, without an abstract position register, drive the edge shutter?
3. Is that native matter gate robust outside one protected controller Hamiltonian?
4. Do independent local and global occupation regulators converge to the same scattering result?
5. Can the outgoing one-photon/vacuum structure be isolated on one undoubled oscillator chain?

6. Can the Hamiltonian be represented by a compact MPO and propagated by a solver independent of the earlier TEBD decomposition?

The experiments distinguish a completed finite-system statement from a continuum or long-chain inference throughout.

2 Matched switch-history references

The autonomous joint Hamiltonian is

$$H_{\text{joint}} = I_C \otimes H_{\text{open}} + P_C \otimes C + H_C \otimes I_F. \tag{1}$$

A final controller outcome records only one late-time label. It does not record the complete function $P_C(t)$ experienced by the field. We therefore extracted three closed-weight histories:

$$p_C^{\text{free}}(t), \qquad p_C^{\text{vac}}(t), \qquad p_C^{\text{pkt}}(t), \tag{2}$$

and evolved field-only references under

$$H_{\text{ref}}(t) = H_{\text{open}} + p_C(t)C. \tag{3}$$

The test uses the unrestricted local tensor product with $N = 6$, local edge dimension $d = 3$, and the complete reduced two-site algebra. The time-dependent references were integrated in a parallel-transport gauge; the largest final norm error is 6.54×10^{-9}.

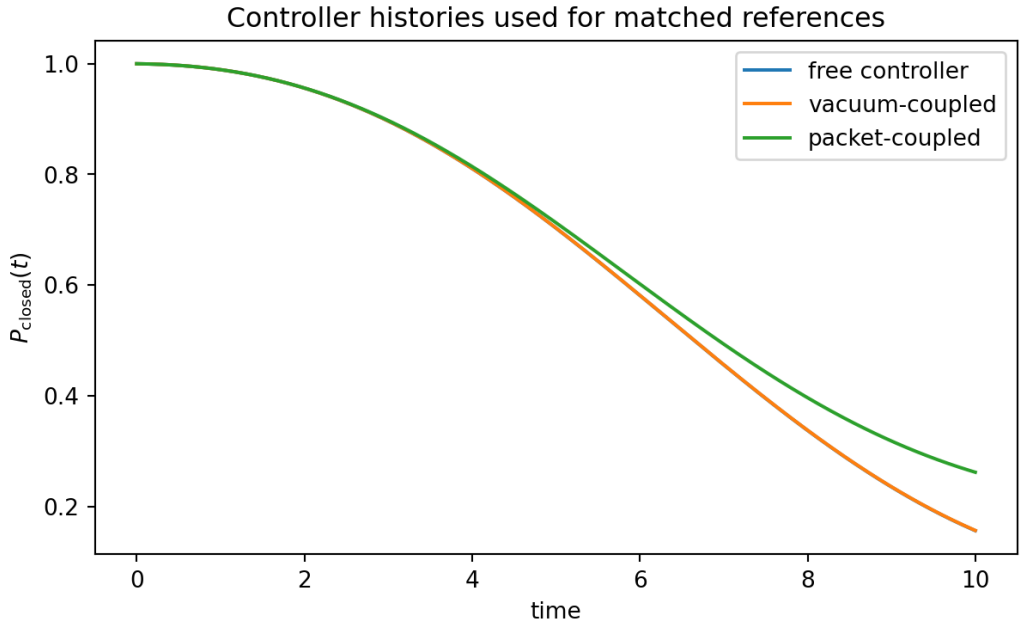

Figure 1: Free, vacuum-coupled, and packet-coupled controller histories used to generate matched field-only references. The packet measurably changes the controller trajectory.

For the far-right open-conditioned packet block,

reference	trace distance
permanently open	0.4039996953
free-controller history	0.0879873101
vacuum-coupled history	0.0880564125
packet-coupled history	0.0948499369

The best reference improves the comparison by a factor

$$\frac{0.4039996953}{0.0879873101} = 4.59157. \tag{4}$$

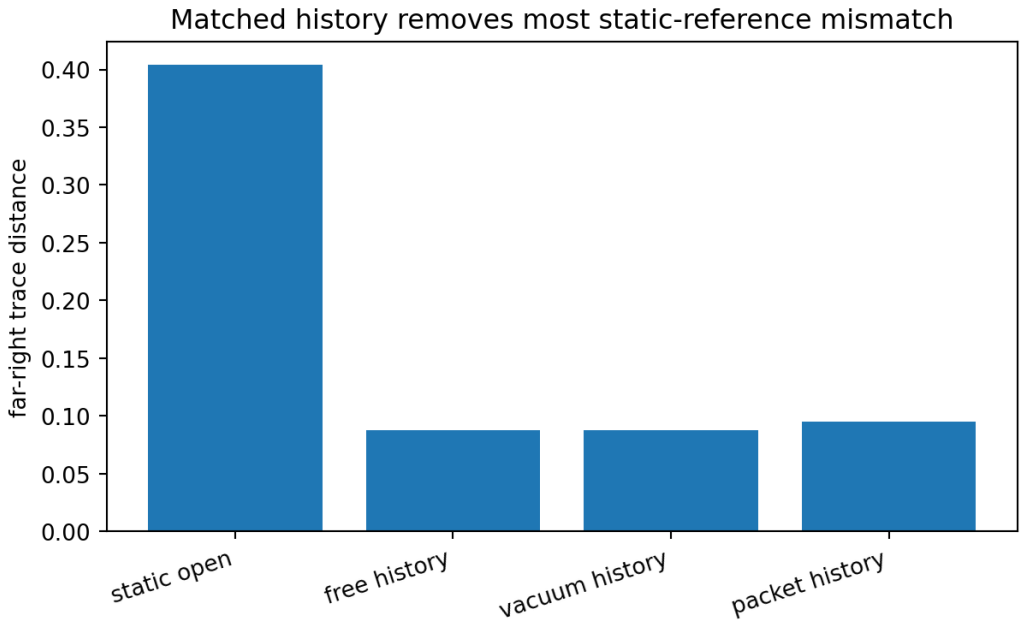

Figure 2: Complete far-right two-site trace distances. A matched mean history removes most, but not all, of the permanently-open mismatch.

The free history is slightly better than the packet-coupled mean history. This is informative rather than paradoxical: conditioning the quantum controller creates branch correlations that cannot be represented by one scalar mean profile. The residual distance is therefore a target for a fluctuation- and branch-resolved reference, not evidence that the history correction failed.

3 Native two-qubit matter controller

The abstract controller is replaced by two ordinary matter qubits. Their standard frustration projector is

$$F = \frac{I - Z_0 Z_1}{2}, \qquad F^2 = F. \tag{5}$$

The native Hamiltonian is

$$H = I_m \otimes H_{\text{open}} + F \otimes C + H_m \otimes I_e, \qquad H_m = \frac{\Omega}{2} X_0. \tag{6}$$

The interaction C is the same direct central edge–edge bilinear already validated in the upgraded exact engine. The canonical run uses $N = 12$, $n_{\max} = 4$, $\Omega = 0.26$, and $T = 20$. The field dimension is 1820 and the joint dimension is 7280.

observable	value
transmission	0.8889371540
total excess occupation	1.0038517905
ΔN_{open}	1.0024229138
packet $\langle F \rangle$	0.8370653342
vacuum $\langle F \rangle$	0.7339882130
controller backaction $\Delta\langle F \rangle$	0.1030771212
packet matter–field entropy	0.2985270740 nats
maximum absolute energy drift	5.93×10^{-11}

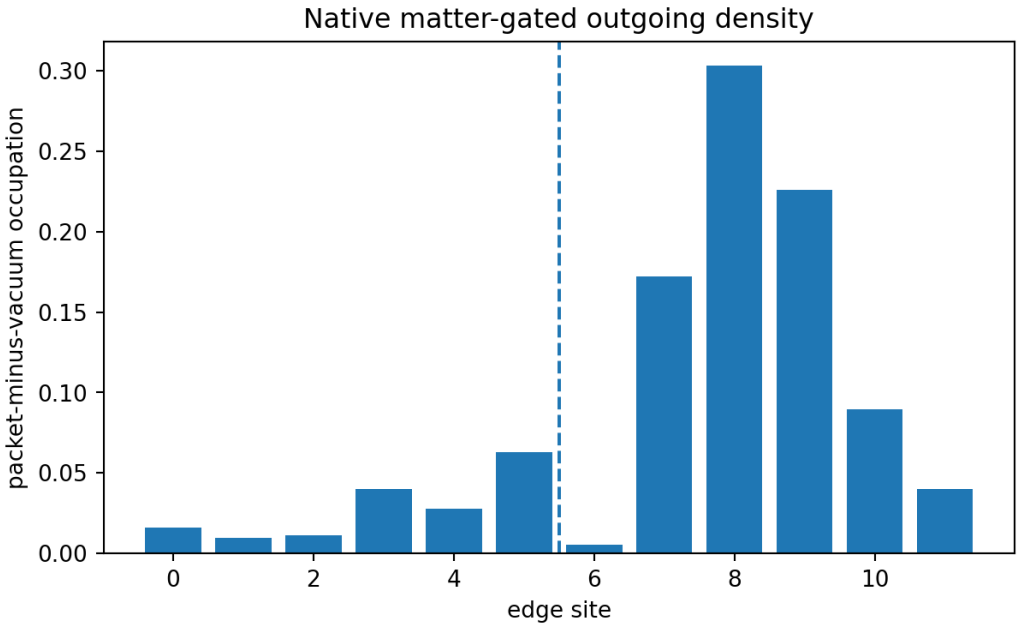

Figure 3: Packet-minus-vacuum edge occupation after native two-qubit matter gating. Most of the outgoing excess lies to the right of the central shutter.

This closes the native controller integration in a minimal matter network. The matter qubits do not merely prescribe a classical function: the packet changes their frustration weight by 0.10308 and generates matter–field entanglement.

3.1 Generic matter-Hamiltonian robustness

Twenty-four cases add transverse and longitudinal one-qubit fields, XX, YY, and ZZ couplings, and coherent initial leakage as large as 0.16. The scan gives

$$0.4724278768 \leq \mathcal{T} \leq 0.7943490510, \qquad \mathrm{median}(\mathcal{T}) = 0.6989478576. \tag{7}$$

The largest absolute energy drift is 7.18×10^{-11}.

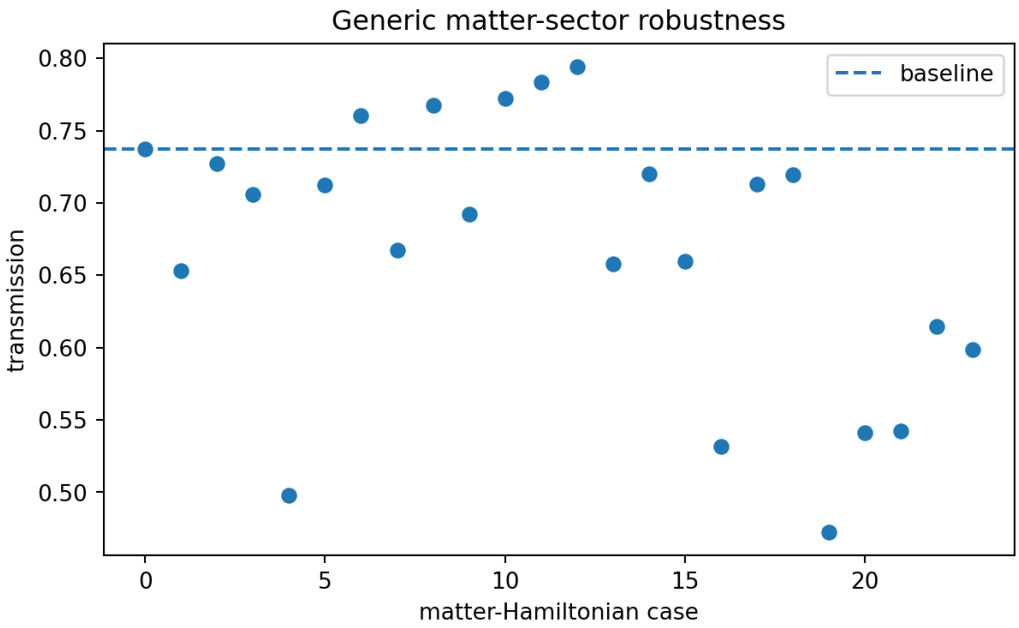

Figure 4: Transmission for the baseline and 23 structured/random matter-sector perturbations. The mechanism survives, while the quantitative routing remains controller-Hamiltonian dependent.

The correct claim is robustness of the gating mechanism, not universal transmission. Different matter Hamiltonians should produce different boundary histories and therefore different scattering.

4 Independent regulator convergence

The global low-occupation basis could, in principle, hide artifacts absent in a true local tensor-product edge Hilbert space. A four-edge benchmark was therefore calculated independently with both regulators.

regulator	cutoff	transmission
local product	$d = 3$	0.2976484664
local product	$d = 4$	0.2918651675
local product	$d = 5$	0.2918268406
local product	$d = 6$	0.2918148483
global occupation	$n_{\max} = 3$	0.2906453482
global occupation	$n_{\max} = 4$	0.2905332479
global occupation	$n_{\max} = 5$	0.2917970497
global occupation	$n_{\max} = 6$	0.2917956999
global occupation	$n_{\max} = 7$	0.2918116362

The final relative difference is 1.10×10^{-5}, while the $d = 6$ maximum top-rung probability is 9.40×10^{-6}.

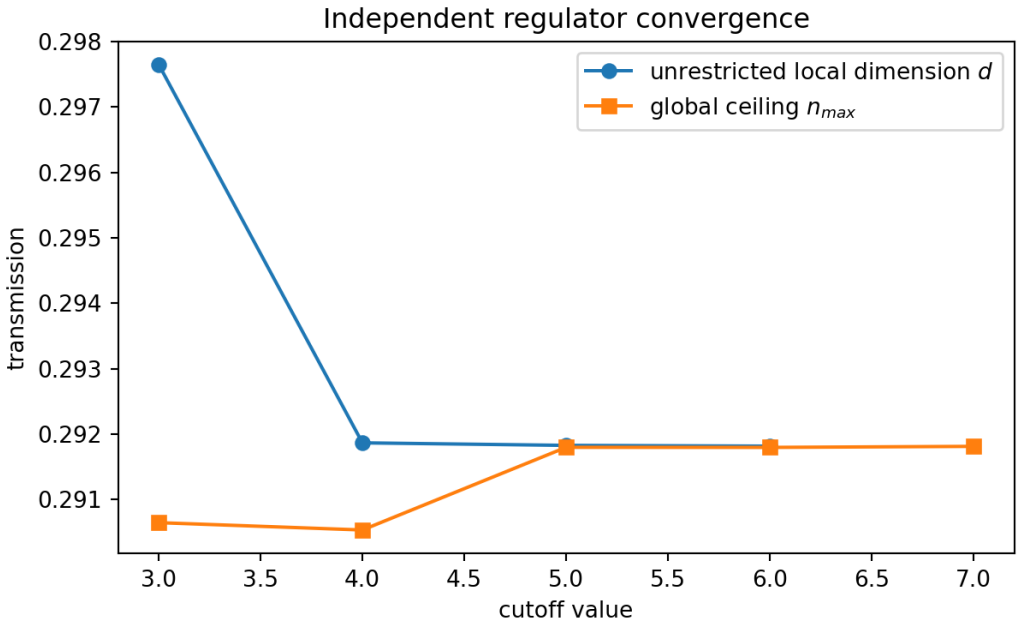

Figure 5: Independent convergence of the unrestricted local-product and global total-occupation regulators.

This comparison does not prove all long-chain projected calculations are converged. It does establish that the two regulators approach the same finite-system scattering answer when both are controllable.

5 Undoubled Gaussian outgoing local algebra

The native oscillator chain was next treated without a Fock cutoff. Before opening, the central spring is absent; after opening, the nearest-neighbour chain is connected. The exact quadratic symplectic map propagates both the closed-vacuum covariance and the one-photon polynomial.

For a local Weyl operator $W(\xi) = \exp(i\xi^T R)$, the evolved one-photon characteristic function has the form

$$\chi(\xi) = \left(1 - |r\xi|^2\right) \exp\left(-\frac{1}{2}\xi^T V \xi\right). \tag{8}$$

On the outgoing half-chain, r was projected onto the open positive-frequency subspace. This gives two controlled comparisons:

1. a matched outgoing mode on the same evolved covariance V, isolating mode mismatch;
2. the same outgoing mode on the permanently open covariance V_{open}, retaining both mode and background/history mismatch.

At $N = 256$, 1200 local probes give

$$\epsilon_{\text{matched}} = 1.18011 \times 10^{-5}, \qquad \epsilon_{\text{open}} = 5.40663 \times 10^{-4}, \tag{9}$$

so the matched construction improves the photon-side RMS error by a factor 45.8145. The vacuum-side matched error is 9.86422×10^{-10}, and the regularized positive-frequency residual is 0.0111433.

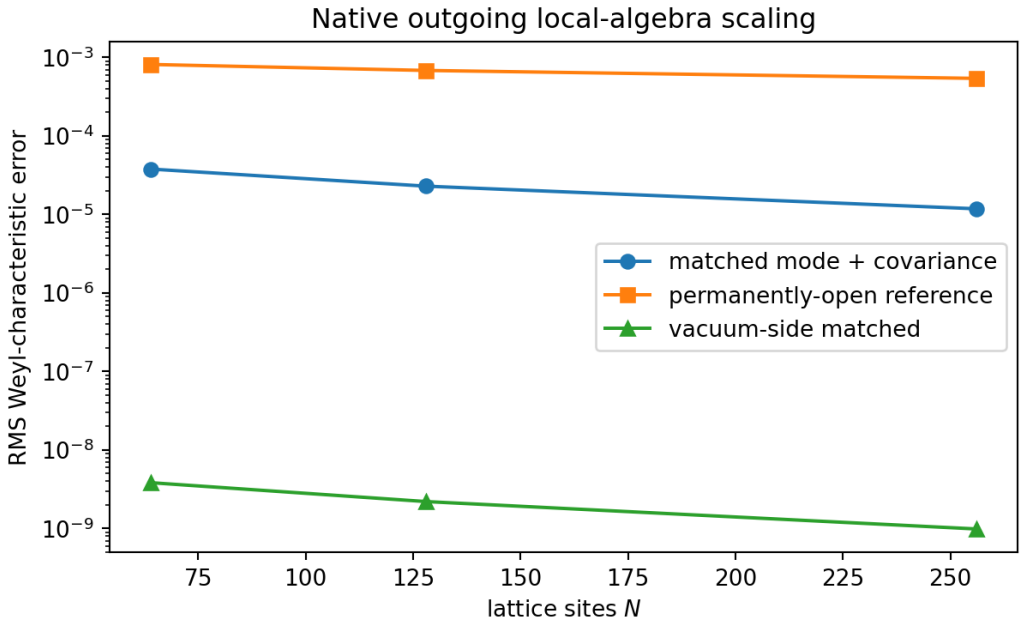

Figure 6: Local Weyl-characteristic errors on the undoubled Gaussian chain. Matching both outgoing mode and covariance isolates a much smaller residual than a permanently-open reference.

The matched-covariance comparison is deliberately not advertised as an independent reconstruction of the state. It isolates the one-photon mode mismatch while holding the Gaussian background fixed. The remaining continuum theorem requires a reference generated independently by the same physical switching law and an explicit asymptotic forward/backward scattering split.

5.1 Finite-Fock validation

The Gaussian one-photon Weyl formula was checked against exact finite-Fock evolution of a two-oscillator shutter. At $d = 10$, 60 probes give RMS error 5.98350×10^{-7} and maximum error 2.66437×10^{-6}.

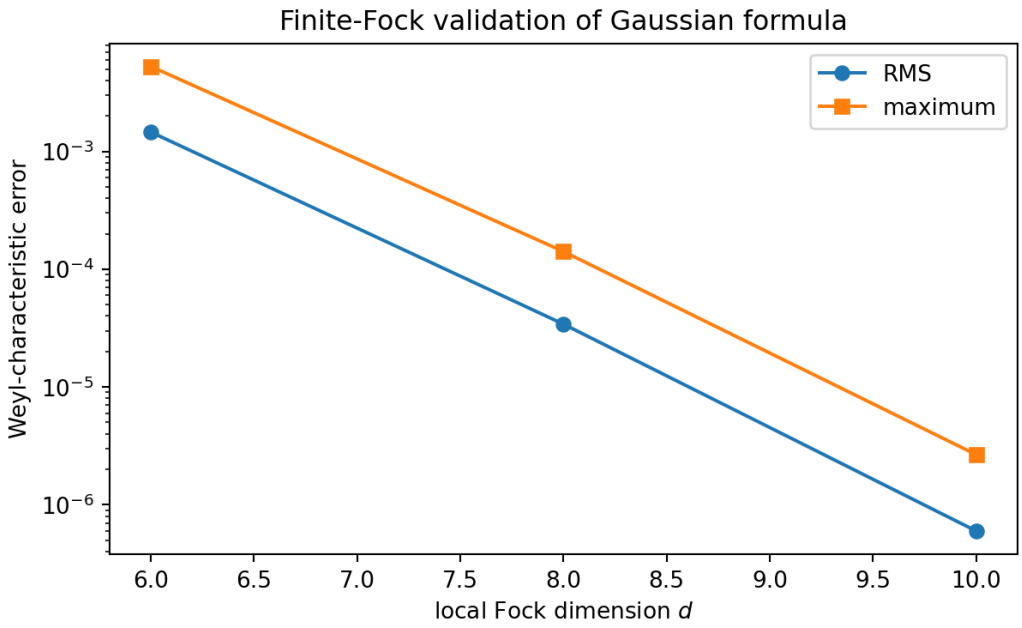

Figure 7: Finite-Fock convergence to the analytic Gaussian one-photon characteristic function.

6 Ultraviolet and smooth-continuum controls

The abrupt perfect-cut vacuum number was calculated for $N = 48$ through 512 and fit to

$$N_{\mathrm{vac}} = A(\log N)^2 + B \log N + C. \tag{10}$$

The fit yields

$$A = 0.0515911280, \qquad R^2 = 0.9999999750. \tag{11}$$

The finite-box coefficient $1/(2\pi^2) = 0.0506605918$ differs by 1.84% over the finite scan.

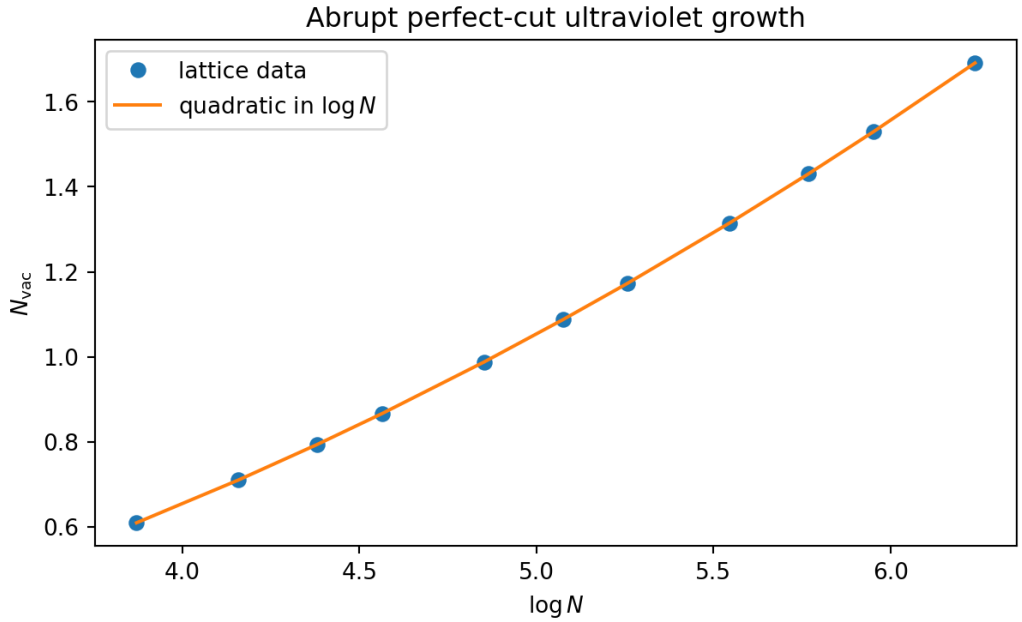

Figure 8: Abrupt perfect-cut particle number and the quadratic-in-log N fit.

This abrupt divergence is not confused with the smooth finite-barrier limit. The controlled Phase-V bridge, included in the reproduction bundle, first converges the native square-root ladder at each spacing and then takes the Gaussian spacing limit. It gives

$$N_{\mathrm{vac}}^{(\infty)} = 0.2084687287, \qquad E_{\mathrm{vac}}^{(\infty)} = 1.0568165290. \tag{12}$$

At the strongest completed native point, the relative native/Gaussian number error is 6.34×10^{-4}.

7 Native outgoing-mode density matrix

The full native matter-gated calculation was also analyzed without replacing it by a Gaussian state. The leading packet-minus-vacuum natural orbital on each spatial region was promoted to an open positive-frequency mode c. Its finite-cutoff reduced density matrix was reconstructed through the normal-ordered identity

$$|0\rangle\langle 0|_c =: \exp(-c^\dagger c) := \sum_{k=0}^{n_{\max}} \frac{(-1)^k}{k!} (c^\dagger)^k c^k. \tag{13}$$

For the right outgoing mode,

$$P(1) = 0.8075107335, \qquad P(n \geq 2) = 1.84966 \times 10^{-4}, \tag{14}$$

and the packet-state trace distance from one photon is 0.1924895190. The corresponding vacuum-run distance from vacuum is 2.67493×10^{-6}.

Conditioning on the final $F = 1$ matter sector gives

$$P(1) = 0.9151647948, \qquad D(\rho_c, |1\rangle\langle 1|) = 0.0848362475. \tag{15}$$

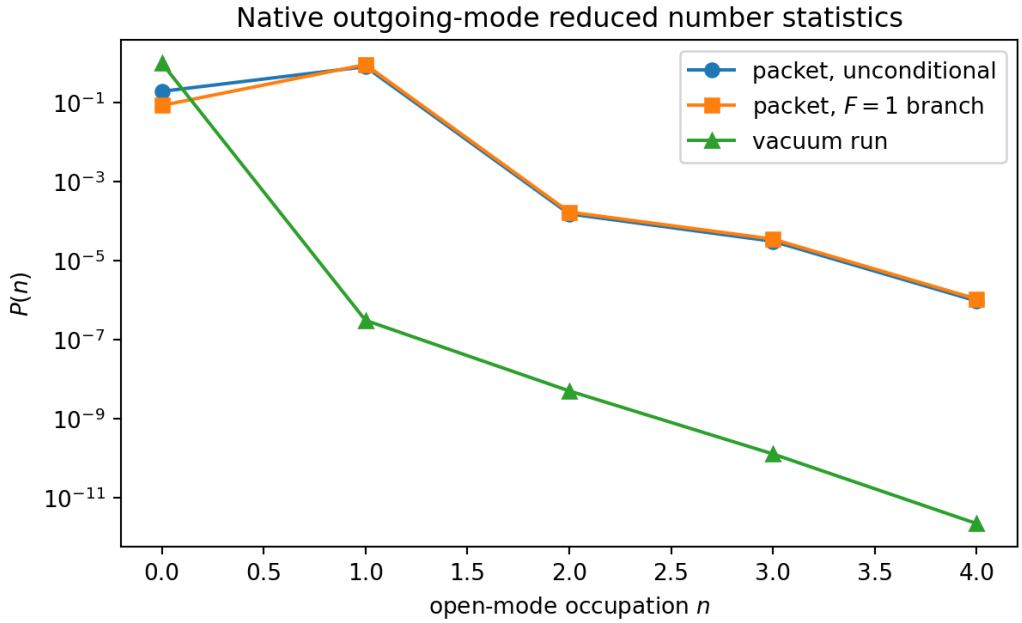

Figure 9: Reduced number statistics for the right positive-frequency mode. The vacuum run is essentially vacuum; the packet run is dominated by one photon with resolved multiparticle weight.

This is a finite standing/open-mode precursor. The final F label is not a full switch-history record, and the mode is not yet an asymptotic scattering packet.

8 Compact MPO-Krylov solver

The entire autonomous Hamiltonian admits a compact bond-dimension-four MPO. In the site ordering with the controller inserted between the central edges, the special path carries

$$q_\ell \left[-\kappa I + \eta\kappa P_C\right] q_r. \tag{16}$$

All onsite oscillator terms, ordinary nearest-neighbour springs, and controller hopping appear in the same MPO. Its action agrees with direct sparse contraction to 7.42×10^{-14}.

A restarted compressed Krylov propagator was validated on the exact $N = 4$, $d = 3$, $R = 3$ Hilbert space:

Δt	Krylov dimension	vacuum fidelity^2	packet fidelity^2
0.30	4	0.9957557320	0.9991112916
0.15	5	0.9999999004	0.9999999334
0.10	6	0.99999999997	0.99999999994

At the strongest point, the phase-aligned packet error is 7.47×10^{-6} and the energy drift is 2.49×10^{-14}.

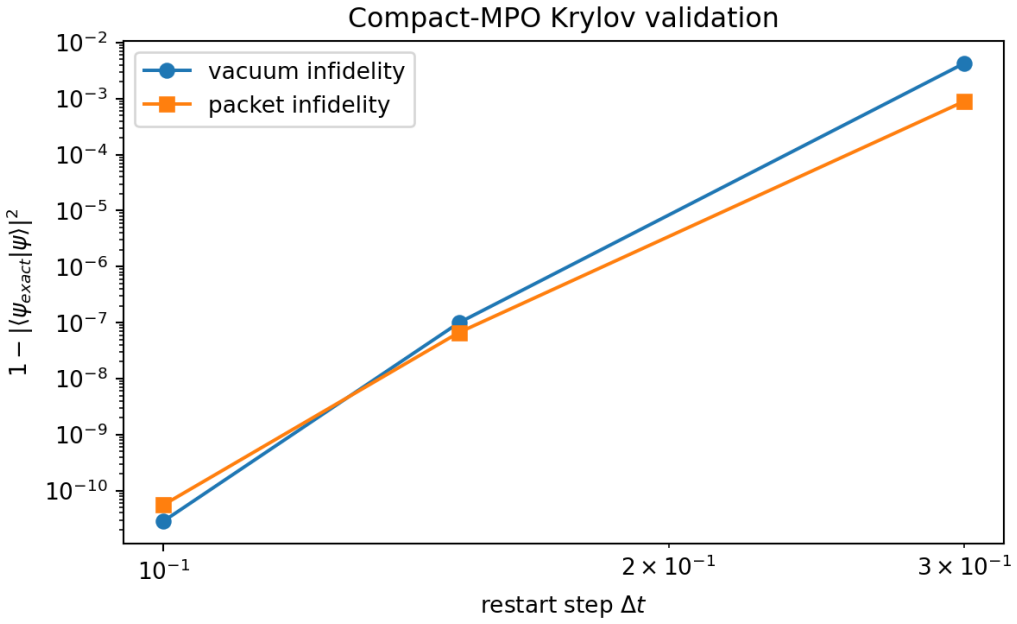

Figure 10: Infidelity of the compact-MPO restarted Krylov propagator against exact exponentiation.

The solver construction is therefore correct at small size. This does not license a long-chain claim. The previous twelve-site TEBD transmissions

$$0.50883, \qquad 0.67410, \qquad 0.45872 \tag{17}$$

for bond dimensions 20, 24, and 28 remain nonmonotonic, compared with projected reference 0.66908. Their truncation proxies are large. The apparent agreement at $\chi = 24$ is not convergence.

9 What is now established

Established finite-system result. A native square-root edge-ladder chain with a direct edge–edge bilinear can be controlled by the ordinary two-qubit QATNU frustration projector under one fixed Hamiltonian. It routes a one-quantum packet, backreacts on and entangles with the matter controller, conserves total energy, and converges across independent edge-Hilbert-space regulators. References with matched switch history and outgoing positive-frequency structure remove most of the former local-algebra mismatch. A compact MPO-Krylov representation reproduces exact small-system dynamics.

The following are not claimed:

- a completed electromagnetic $U(1)$ derivation from the substrate;
- an asymptotic forward/backward theorem on the same native matter-controlled long chain;
- a converged long-time MPS scattering result;
- a continuum limit taken before the local edge occupation cutoff is controlled;
- equivalence of a final matter/controller label to the complete boundary history.

10 Next decisive integrations

The next calculation should combine all controlled ingredients rather than add another separate module:

1. evolve the compact MPO with systematic χ, local dimension, restart-step, and Krylov-dimension convergence to a full scattering time;
2. place the smooth finite barrier and the two-qubit matter controller in that same long native chain;
3. construct asymptotic right- and left-moving packets from the native chain's scattering modes and trace the backward packet sector explicitly;
4. repeat the local Weyl-algebra test against an independently generated matched-history reference rather than a shared-covariance diagnostic;
5. take the sequential continuum limit: local edge cutoff first at every lattice spacing, spacing second;
6. decompose the residual matched-history distance into controller-field entanglement, profile fluctuations, and positive-frequency fitting error.

The compact MPO is the enabling technical result for this next phase, but its long-time convergence must be demonstrated rather than assumed.

Reproducibility

The accompanying bundle contains source code, raw JSON data, all figures, carried Phase-V continuum and TEBD controls, a concise manuscript insertion, and SHA-256 checksums. The main new scripts reproduce the matched-history experiment, native matter gate, generic matter scan, regulator comparison, Gaussian outgoing analysis, finite-Fock Weyl validation, native outgoing-mode reduction, and small-system MPO-Krylov validation.